A highly hydrophobic metal-organic framework Zn(BDC)(TED)0.5 for adsorption and separation of CH3OH/H2O and CO 2/CH4: An integrated experimental and simulation study

ARTICLE *in* THE JOURNAL OF PHYSICAL CHEMISTRY C · APRIL 2010

Impact Factor: 4.77 · DOI: 10.1021/jp1003177

A Highly Hydrophobic Metal−Organic Framework $Zn(BDC)(TED)_{0.5}$ for Adsorption and Separation of CH_3OH/H_2O and CO_2/CH_4: An Integrated Experimental and Simulation Study

Y. F. Chen,[†] J. Y. Lee,[‡] R. Babarao,[†] J. Li,[‡] and J. W. Jiang[†,*]

Department of Chemical and Biomolecular Engineering, National University of Singapore, 117576, Singapore and Department of Chemistry and Chemical Biology, The State University of New Jersey, Piscataway, New Jersey 08854

Received: January 12, 2010; Revised Manuscript Received: March 2, 2010

The adsorption and separation of CH_3OH/H_2O and CO_2/CH_4 in $Zn(BDC)(TED)_{0.5}$ (BDC = benzenedicarboxylate, TED = triethylenediamine) are investigated by integrating experiment and simulation. $Zn(BDC)(TED)_{0.5}$ is a highly hydrophobic metal−organic framework (MOF) with interlacing channels. The simulated isotherms of CH_3OH and H_2O are in fairly good agreement with experimental results. While H_2O adsorption in $Zn(BDC)(TED)_{0.5}$ is vanishingly small, CH_3OH shows a much stronger adsorption. The selectivity of CH_3OH over H_2O is approximately 20 at low pressures and the selectivity decreases with increasing pressure. From the density distributions and structural analysis, it is found that CH_3OH interacts strongly with the metal oxides, particularly at low pressures. The isotherms of CO_2 and CH_4 from simulation match well with experimental data. As a nonpolar molecule, CO_2 exhibits different favorable sites from polar CH_3OH. At low pressures, CO_2 is located preferentially near the BDC linkers. As pressure increases, CO_2 is proximal to the metal oxides and TED linkers. The selectivity of CO_2 over CH_4 increases as a function of pressure, with a magnitude similar to that in most neutral MOFs. H_2O has a negligible effect on the selectivity of CO_2/CH_4. In addition, the simulated adsorption isotherm of *n*-hexane is in accord with experiment. This work provides a quantitative understanding at the molecular level for adsorption behavior in $Zn(BDC)(TED)_{0.5}$ and suggests that $Zn(BDC)(TED)_{0.5}$ is a good candidate for the separation of alcohol/water mixtures and alcohol-based liquid fuels.

1. Introduction

As a unique class of hybrid nanoporous materials, metal−organic frameworks (MOFs) have attracted considerable interest in recent years.[1,2] Composed of the tunable metal clusters and organic linkers, MOFs possess extremely large surface areas and well-defined pores, and are regarded as promising candidates for storage, separation, catalysis, and other emerging applications.[3−5] A large number of experimental and simulation studies have been reported for the storage of energy carriers H_2 and CH_4 and greenhouse gas CO_2. For example, isoreticular MOFs (IRMOFs) with different organic groups were examined for CH_4 storage.[6] CO_2 adsorption was determined in a series of MOFs and MOF-177 was found to exhibit a high capacity of CO_2 up to 33 mmol/g.[7] Adsorption of various gases in MOFs was simulated and compared with experimental data to test the validity of proposed atomic models.[8,9] H_2 uptake in IRMOFs from simulations was found to correlate well with isosteric heat at low pressures, with surface area at moderate pressures, and with free volume at high pressures.[10] There has also been considerable interest in the use of MOFs for the removal of CO_2 from natural gas. The adsorption and selectivity of CO_2/CH_4 mixtures were simulated in IRMOF-1 and Cu-BTC.[11,12] Carborane-based MOFs in the presence and absence of exposed metal sites were examined for the separation of CO_2/CH_4 mixtures, and a higher selectivity was observed in the former case.[13] Unprecedentedly high selective adsorption was predicted for CO_2/CH_4 and other industrially important gas mixtures in both cationic and anionic MOFs.[14,15]

Recently, a novel MOF named $Zn(BDC)(TED)_{0.5}$ (BDC = benzenedicarboxylate, TED = triethylenediamine) was synthesized and characterized.[16,17] It is thermally stable up to 282 °C, readily activated, and highly porous (61.3%). H_2 sorption capacity in $Zn(BDC)(TED)_{0.5}$ is exceptionally high, up to 2.1 wt % at 78 K and 1 bar. In addition, $Zn(BDC)(TED)_{0.5}$ is highly hydrophobic and adsorbs a large amount of hydrocarbons giving the highest capacities among all MOFs reported to date.[17] Attributed to these salient features, several studies have been subsequently carried out in $Zn(BDC)(TED)_{0.5}$. Using experimental and simulation methods, the adsorption and diffusion of H_2 were examined up to 50 bar at 77 and 298 K.[18] The siting and segregation of complex alkane mixtures were simulated, which suggested a new possibility for the design and creation of highly selective adsorption sites in MOFs.[19] The adsorption of hexane isomers was studied and compared with experimental results.[20] The diffusion of binary mixtures was studied in $Zn(BDC)(TED)_{0.5}$, other MOFs, and zeolites by a unified Maxwell−Stefan description, which is convenient for use in engineering design of separation and reaction systems in porous materials.[21]

In this work, we integrate experimental and simulation techniques to examine the adsorption and separation of CH_3OH/H_2O and CO_2/CH_4 mixtures in $Zn(BDC)(TED)_{0.5}$. The objective is to provide the microscopic understanding of adsorption behavior in this novel MOF at a molecular level. The study is technologically important regarding the capability of $Zn(BDC)(TED)_{0.5}$ in the purification of alcohol/water mixture and natural gas. The removal of H_2O from alcohol and of CO_2 from natural gas is crucial to their efficacy in combustion. We compare the experimental and simulated adsorption isotherms of single-component CH_3OH, H_2O, CO_2, and CH_4, and predict the adsorption of mixtures. The effect of H_2O on the separation of

* To whom correspondence should be addressed. Phone: +65 65165083. Fax: +65 67791936. E-mail: chejj@nus.edu.sg.
[†] Department of Chemical and Biomolecular Engineering.
[‡] Department of Chemistry and Chemical Biology.

10.1021/jp1003177
Published on Web 03/17/2010

CO_2/CH_4 mixture is examined. As mentioned, Zn(BDC)(TED)$_{0.5}$ shows the highest adsorption for hydrocarbons of all other MOFs reported; consequently, the adsorption of *n*-hexane (*n*-C_6) is also simulated in Zn(BDC)(TED)$_{0.5}$. To provide the microscopic understanding of adsorption, the density distributions and structural properties of adsorbates in Zn(BDC)(TED)$_{0.5}$ are presented from simulations.

2. Experimental Materials and Methods

2.1. Preparation of Zn(BDC)(TED)$_{0.5}$. The g-scale and single crystal of Zn(BDC)(TED)$_{0.5}$ has been synthesized based on previously reported procedures but with some modifications.[17] The slightly modified route involves higher temperature (150 °C) and shorter reaction time (1 day), which leads to better crystallinity and higher yield. Initially, a mixture of zinc(II) nitrate tetrahydrate (1.464 g, 5.6 mmol), H_2BDC (0.960 g, 5.8 mmol), TED (0.432 g, 3.9 mmol), and 120 mL of DMF was loaded in a 250 mL beaker. After mixing of all chemicals, the solution became a cloudy suspension and nitric acid was then added at an approximate ratio of one drop per 10 mL of DMF solution. An ultrasonic treatment was given to dissolve all solids until a clear solution formed (in a warm tap water bath). The solution was then transferred to an acid digestion bomb and heated at 150 °C for 1 day. Colorless single crystals of [Zn(BDC)(TED)$_{0.5}$]·2DMF·0.2H_2O were isolated after filtering and washing with 10 mL of DMF three times and drying under vacuum at 50 °C in gram scale (2.152 g, 89% yield). The guest-free sample was prepared by activation at 100 °C for 18 h under vacuum to remove DMF and water. The structural integrity of Zn(BDC)(TED)$_{0.5}$ was confirmed by Powder X-ray Diffraction (PXRD) study as described previously.[17]

2.2. Isotherms of CO_2, CH_4, CH_3OH, and H_2O. The high pressure CO_2 and CH_4 isotherms were experimentally collected using a high pressure adsorption analyzer, HPVA-100 (VTI Corp.). Each isotherm was obtained separately and NIST gas behavior model was given for data analyses with automated software HPA (VERSION 11). The pressures of manifold and the sample cell were monitored by two electronic Bourdon gauge-type transducers (Mensor), separately. The transducers could read the pressure to 1500 psi with 0.010% accuracy. The high vacuum ($\sim 10^{-6}$ mbar) was controlled by a turbomolecular pump from Pfeiffer. Ultrahigh purity He (UHP 5.0) was used to determine dead space of the sample cell and high purity CO_2 (research grade 4.5) and CH_4 (UHP 4.0) were used for analysis, respectively. About 600 mg of activated sample of Zn(BDC)(TED)$_{0.5}$ was used for high pressure gas sorption analysis. The ambient temperature was controlled by a computer-controlled water bath from Polyscience Co. The CH_3OH and H_2O adsorption experiments were carried out on a computer-controlled DuPont Model 990 TGA. The partial pressures of CH_3OH and H_2O were varied by changing the blending ratios of adsorbate-saturated nitrogen and pure nitrogen gas streams. The Zn(BDC)(TED)$_{0.5}$ samples were activated at 120 °C.

3. Simulation Models and Methods

Zn(BDC)(TED)$_{0.5}$ possesses a paddle-wheel structure, in which the metal−oxides $Zn_2(COO)_4$ are bridged by BDC linkers to form a 2D square-grid net [Zn_2(1,4-BDC)$_2$]. The TED pillars occupy the axial sites to extend the 2D layers into a 3D framework and they are disordered along the crystallographic 4-fold axis. The structure belongs to space group P_4/mmm, with lattice constants of $a = 10.929$ Å and $c = 9.608$ Å. Figure S1 of the Supporting Information shows the crystal structure ($3 \times 3 \times 3$ unit cells) constructed from experimental crystallographic data and first-principles optimization. The optimization was conducted on a unit cell of Zn(BDC)(TED)$_{0.5}$ by the periodical density functional theory (DFT), using DMol3.[22] The Becke exchange plus Lee−Yang−Parr functional and the double-ξ numerical polarization (DNP) basis set were used in the DFT optimization. The DNP basis set incorporates d-type polarization into heavier atoms and p-type polarization into hydrogen atoms, and is comparable to the 6-31G(d,p) Gaussian-type basis set. The effective core potentials were adopted, which represent the interactions of nucleus and core electrons on the valence electrons. In such a way only the wave functions of the softer valence electrons are explicitly treated, which usually controls the chemistry, and can significantly reduce computational cost.

There exist interlacing channels in the framework of Zn(BDC)(TED)$_{0.5}$. Figure 1 shows the morphologies and diameters of the channels calculated with the HOLE program.[23] The wide open channels are along the *Z* axis with a diameter ranging from 7.3 to 9.2 Å, which are connected by the small windows along the *X* and *Y* axes with a diameter of 3.6 Å. Therefore, small molecules may enter into the windows. The free volume V_{free} of Zn(BDC)(TED)$_{0.5}$ was evaluated from Monte Carlo simulation[24] with helium as a probe. The V_{free} was estimated to be 0.79 cm^3/g; the porosity was 64.9%, in good agreement with the experimental accessible volume (61.3%).[17]

The atomic charges of the framework atoms in Zn(BDC)(TED)$_{0.5}$ were calculated from DFT. Because of the large number of atoms in a unit cell, a fragmental cluster shown in Figure S2 (Supporting Information) was used. The dangling bonds on the fragmental cluster were terminated by hydrogen atoms. The DFT calculation used the Becke exchange plus Lee−Yang−Parr functional and was carried out with Gaussian 03.[25] The 6-31G(d) basis set was used for all atoms except Zn atoms, for which the LANL2DZ basis set was used. LANL2DZ is a double-ζ basis set and contains effective pseudopotentials to represent the potentials of nucleus and core electrons. The atomic charges were estimated by fitting to the electrostatic potentials.[26] The dispersion interactions of the framework atoms in Zn(BDC)(TED)$_{0.5}$ were modeled by the DREIDING force field,[27] which has been commonly adopted in the simulation of MOFs.

H_2O was mimicked by the three-point transferable interaction potentials (TIP3P) model,[28] in which the O−H bond length was 0.9572 Å and the ∠HOH angle was 104.52°. It has been shown that the TIP3P model gives a reasonably good interaction potential compared to the experimental value.[29] CO_2 was represented as a three-site rigid molecule and its intrinsic quadrupole moment was described by a partial-charge model.[30] The partial charges on C and O atoms were $q_C = 0.576e$ and $q_O = -0.288e$ ($e = 1.6022 \times 10^{-19}$ is the elementary charge), respectively. The C−O bond length was 1.18 Å and the bond angle O−C−O was 180°. The intermolecular interactions of H_2O and CO_2 were modeled by the additive LJ and Coulombic potentials

$$u_{ij}(r) = \sum_{\substack{\alpha \in i \\ \beta \in j}} \left\{ 4\varepsilon_{\alpha\beta}\left[\left(\frac{\sigma_{\alpha\beta}}{r_{\alpha\beta}}\right)^{12} - \left(\frac{\sigma_{\alpha\beta}}{r_{\alpha\beta}}\right)^{6}\right] + \frac{q_\alpha q_\beta}{4\pi\varepsilon_0 r_{\alpha\beta}} \right\} \quad (1)$$

where $\varepsilon_0 = 8.8542 \times 10^{-12}$ C^2 N^{-1} m^{-2} is the permittivity of the vacuum, and $\sigma_{\alpha\beta}$ and $\varepsilon_{\alpha\beta}$ are collision diameter and potential well depth, respectively. CH_3OH, CH_4, and *n*-C_6 were represented by the united-atom models with CH_x as a single interaction site. The potential parameters were adopted from the transferable potentials for phase equilibria (TraPPE) force field, developed to reproduce the critical parameters and saturated liquid densities of alkanes and alcohols.[31,32] In addition

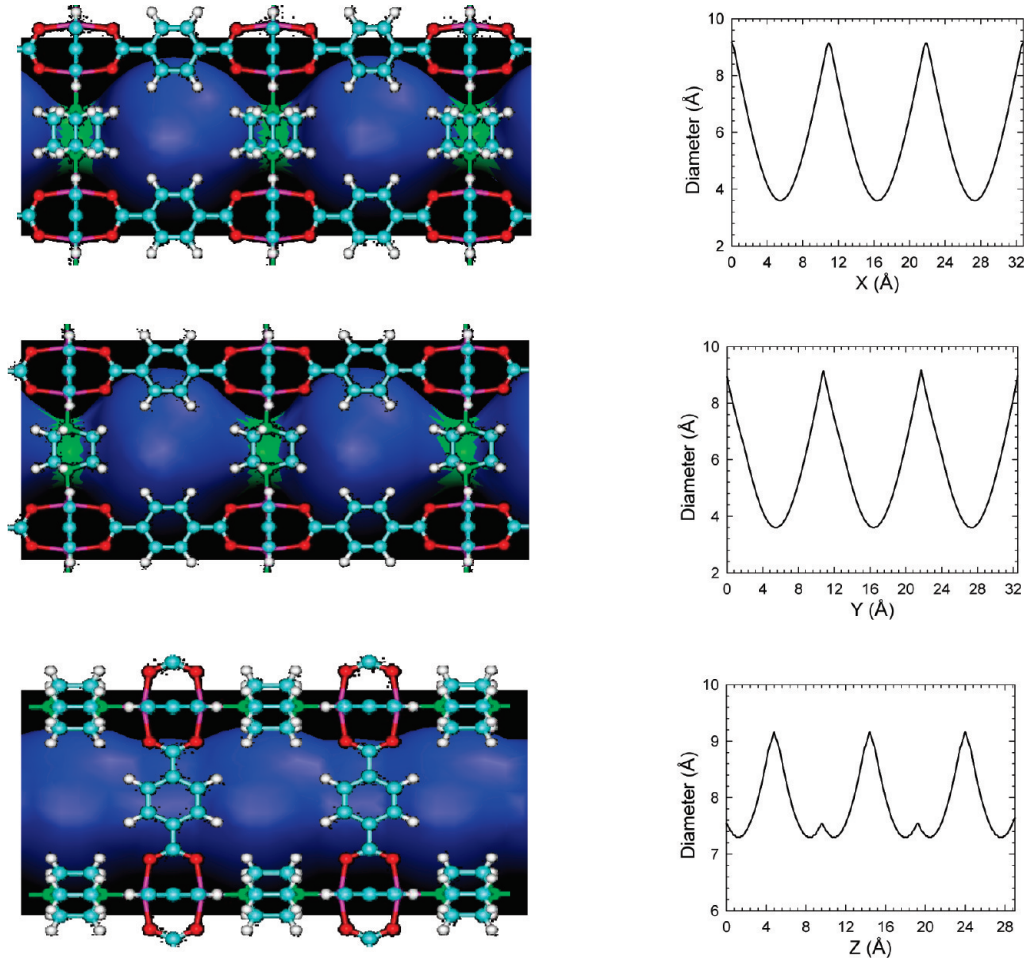

Figure 1. Channel morphologies and diameters along the *X*, *Y*, and *Z* (from top to bottom) axes in $Zn(BDC)(TED)_{0.5}$. The green regions denote the small windows.

TABLE 1: Potential Parameters for Adsorbates H_2O, CO_2, CH_4, CH_3OH, and *n*-C_6

		LJ and Coulombic potential				
species	site	σ (Å)	ε/k_B (K)	q (e)	bond length	bending angle and force constant
CH_4	CH_4	3.73	148.0	0		
CO_2	C	2.789	29.66	+0.576	$r_{C-O} = 1.18$ Å	$\theta_{\angle OCO} = 180°$
	O	3.011	82.96	−0.288		
H_2O	O	3.151	76.47	−0.834	$r_{H-O} = 0.9527$ Å	$\theta_{\angle HOH} = 104.52°$
	H	0	0	+0.417		
CH_3OH	CH_3	3.75	98.0	+0.265	$r_{CH_3-O} = 1.43$ Å	$\theta_{\angle CH_3OH} = 108.5°$
	O	3.02	93.0	−0.700	$r_{O-H} = 0.945$ Å	$k_\theta/k_B = 55400$ K
	H	0	0	+0.435		
n-C_6	CH_3	3.75	98.0	0	$r_{CH_x-CH_y} = 1.54$ Å	$\theta_{CH_x-CH_2-CH_y} = 113.0°$
	CH_2	3.95	46.0	0		$k_\theta/k_B = 62500$ K

to the LJ interaction (and the Coulombic interaction for CH_3OH), there were bending interactions in CH_3OH and *n*-C_6

$$u_{\text{bending}}(\theta) = 0.5k_\theta(\theta - \theta_0)^2 \quad (2)$$

Table 1 lists the potential parameters for adsorbates CH_3OH, H_2O, CO_2, CH_4, and *n*-C_6. Furthermore, the torsion interaction was also taken into account for *n*-C_6

$$u_{\text{torsion}}(\phi) = c_0 + c_1[1 + \cos\phi] + c_2[1 - \cos(2\phi)] + c_3[1 + \cos(3\phi)] \quad (3)$$

where $c_0/k_B = 0$, $c_1/k_B = 355.03$, $c_2/k_B = 68.19$, and $c_3/k_B = 791.32$.

Grand canonical Monte Carlo (GCMC) simulations were carried out for the adsorption of pure components and mixtures in $Zn(BDC)(TED)_{0.5}$. Because the chemical potentials of adsorbate in adsorbed and bulk phases are identical at thermodynamic equilibrium, GCMC simulation allows one to relate the chemical potentials of adsorbate in both phases and has been widely used to simulate adsorption. The framework atoms in $Zn(BDC)(TED)_{0.5}$ were assumed to be rigid and the potential energies between adsorbate atoms and framework were pretabulated. This is because the low-energy equilibrium configurations are involved in adsorption and the flexibility of framework has only a marginal effect. A recent simulation study on the adsorption of noble gases in IRMOF-1 demonstrated that rigid and semiflexible frameworks gave close results at both low and room temperatures.[33] The LJ interactions were evaluated with a spherical cutoff of 13 Å with the long-range corrections added;

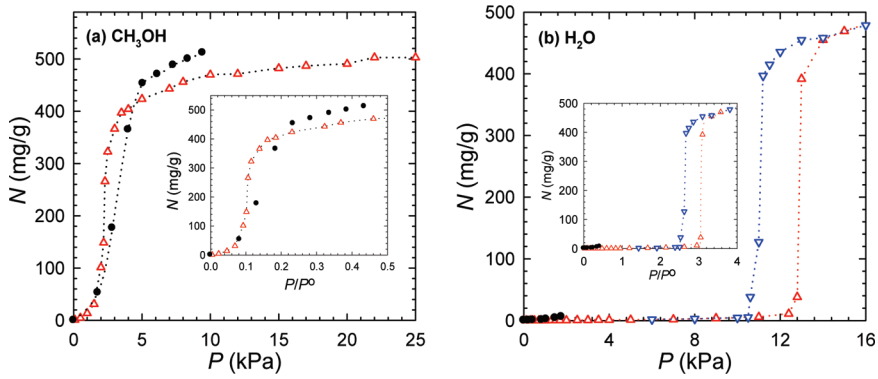

Figure 2. Isotherms of single-component CH_3OH and H_2O at 303 K as a function of pressure. The filled circles are experimental data. The upper and lower triangles are adsorption and desorption data from simulation. The insets show the isotherms as a function of reduced pressure. The saturation pressure P^o is 21.7 kPa for CH_3OH and 4.2 kPa for H_2O.

the Coulombic interactions were calculated by using the Ewald summation. The real/reciprocal space partition parameter and the cutoff for reciprocal lattice vectors were chosen to be 0.2 $Å^{-1}$ and 8, respectively, to ensure the convergence of Ewald sum. The number of trial moves in a typical GCMC simulation was 2×10^7, though additional trial moves were used at high pressures. The first 10^7 moves were used for equilibration and the second 10^7 moves for ensemble averages. Five types of trial moves were randomly attempted in the GCMC simulation: displacement, rotation, and partial regrowth at a neighboring position; entire regrowth at a new position; and swap with reservoir including creation and deletion at equal probability. For mixtures, another type of trial move, the exchange of molecular identity, was also included. Unless otherwise mentioned, the simulation uncertainties were smaller than the symbol sizes presented below.

4. Results and Discussion

4.1. CH_3OH/H_2O. Figure 2 shows the isotherms of single-component CH_3OH and H_2O in $Zn(BDC)(TED)_{0.5}$ at 303 K. The experimental and simulated isotherms are in fairly good agreement, particularly for CH_3OH at low pressures and for H_2O over the pressure range under study. Note that the saturation pressure is 21.7 kPa for CH_3OH and 4.2 kPa for H_2O.[34] With increasing pressure, the uptake of CH_3OH increases sharply until $P/P^o = 0.2$ and finally approaches a plateau. The simulation underestimates the saturation loading of CH_3OH. Specifically, the predicted saturation loading is approximately 460 mg/g, lower than the experimental value of 510 mg/g.[17] This might imply that the force field used to model the interactions of CH_3OH-CH_3OH and CH_3OH-adsorbent might not be very accurate, and the agreement could be improved by more sophisticated modeling. H_2O uptake from simulation is negligible at $P/P^o < 3.0$, which is consistent with experimental data up to $P/P^o = 0.4$. Interestingly, a hysteresis is observed in the adsorption and desorption isotherms of H_2O at P/P^o within 2.6 and 3.1, indicating the occurrence of capillary phase transition. $Zn(BDC)(TED)_{0.5}$ is a highly hydrophobic framework with the BDC and TED linkers surrounding the metal oxides; therefore, the interaction with H_2O is very weak. It is instructive to note that the behavior of H_2O in $Zn(BDC)(TED)_{0.5}$ is significantly different from that in a hydrophilic MOF. Our recent study revealed that H_2O is strongly adsorbed in cation-exchanged *rho*-ZMOFs because of the high affinity of ionic framework and extraframework ions.[35] H_2O in *rho*-ZMOFs exhibits a three-step adsorption mechanism. At low pressures, H_2O is preferentially adsorbed onto the extraframework ions; with increasing pressure, adsorption occurs near the framework and finally in the large cage.

Figure 3 shows the density contours of CH_3OH in $Zn(BDC)(TED)_{0.5}$ at 1 and 10 kPa, respectively. On the *XY* plane, CH_3OH molecules exclusively occupy the open square channels. Nevertheless, the adsorption sites in the channels are not homogeneous due to the asymmetrical locations of the ethylene ($-CH_2-CH_2-$) fragments in TED linkers. On the basis of the density of adsorbate, three favorable sites (I, II, and III) are identified. Site I is at the framework corner and proximal to the metal oxides. CH_3OH experiences strong interaction at site I with the metal oxides and the overlap of surface potentials. Compared to site I, sites II and III are less favorable. This is because the steric hindrance of the TED linkers prevents CH_3OH at sites II and III from being near the metal oxides. It is clearly seen on the *XZ* and *YZ* planes that the distribution of CH_3OH is extended along the *Z* axis. CH_3OH is also located near the small windows. With increasing pressure from 1 to 10 kPa, the density distribution in the square channels appears less inhomogeneous and the small windows are partially occupied. Nevertheless, the density in the small windows is very low.

The observed change in the density contours with increasing pressure can be further elucidated from the radial distribution functions $g(r)$ of CH_3OH around the typical framework atoms. The $g(r)$ was calculated by

$$g_{ij}(r) = \frac{\Delta N_{ij}(r, r + \Delta r)V}{4\pi r^2 \Delta r N_i N_j} \tag{4}$$

where r is the distance between species i and j, $\Delta N_{ij}(r,r + \Delta r)$ is the number of species j around i within a shell from r to $r + \Delta r$, V is the system volume, and N_i and N_j are the numbers of species i and j. As shown in Figure 4, the peak height in the $g(r)$ around Zn and N atoms increases when pressure increases from 1 to 10 kPa. This indicates that CH_3OH molecules are located closer to the metal oxides at 10 kPa, particularly for molecules at sites II and III. Consequently, the density difference among the three types of adsorption sites reduces and the distribution tends to be homogeneous, as observed in Figure 3. Compared to the case at 1 kPa, CH_3OH molecules also stay near the BDC linkers at 10 kPa, evidenced by the rising peak height at $r = 5.0$ Å in the $g(r)$ around C2 atoms. This correlates with the increase in the $g(r)$ around Zn and N atoms. Nevertheless, the peak height in the $g(r)$ around C4 atoms remains essentially unchanged.

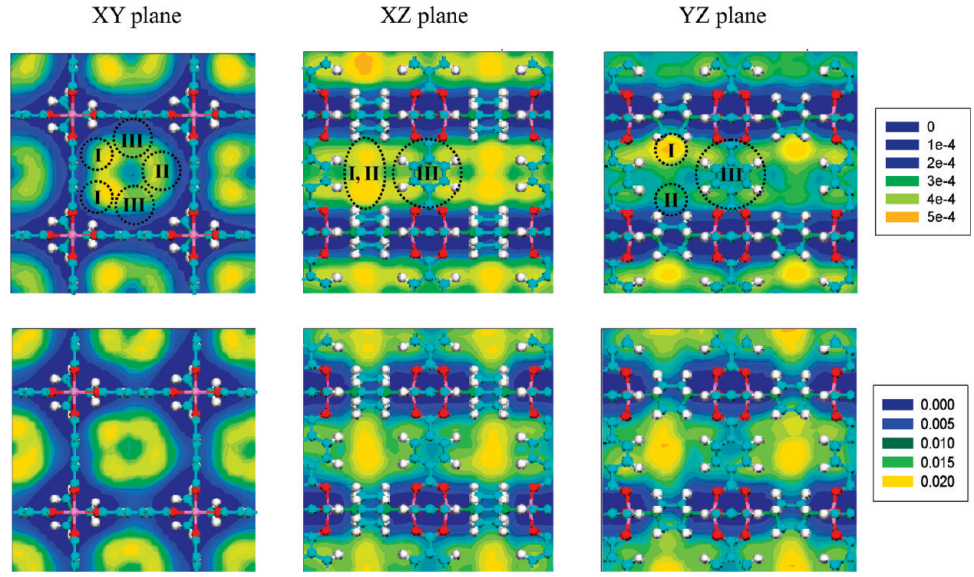

Figure 3. Density contours of CH_3OH at 1 kPa (top) and 10 kPa (bottom). The scale is based on the number of molecules per $Å^3$.

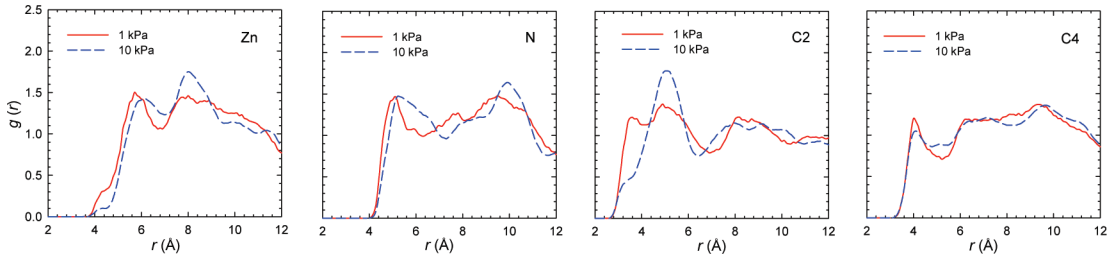

Figure 4. Radial distribution functions of CH_3OH around Zn, N, C2, and C4 atoms of $Zn(BDC)(TED)_{0.5}$ at 1 and 10 kPa. The C2 and C4 atoms are in the BDC and TED linkers, respectively.

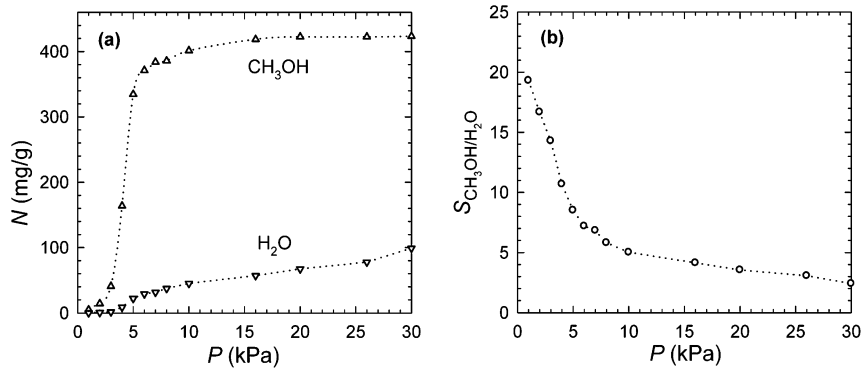

Figure 5. (a) Adsorption and (b) selectivity of an equimolar mixture of CH_3OH/H_2O at 303 K.

The adsorption of an equimolar mixture of CH_3OH/H_2O from simulation is shown in Figure 5a. Note that the mixture could be a vapor or liquid phase under the pressure range. The loading of CH_3OH is much higher than that of H_2O as the hydrophobic framework has a stronger interaction with CH_3OH. In contrast to the negligible adsorption of pure H_2O, an appreciable amount of H_2O is adsorbed from the CH_3OH/H_2O mixture. This is because of the coadsorption between H_2O and already adsorbed CH_3OH. More specifically, the relatively large amount of CH_3OH adsorbed induces strong attraction for H_2O. As a consequence, the adsorption of H_2O in the CH_3OH/H_2O mixture is enhanced upon comparison with pure H_2O. The separation factor of a binary mixture is usually quantified by the adsorption selectivity $S_{ij} = (x_i/x_j)(y_j/y_i)$, where x_i and y_i are the mole fractions of component i in adsorbed and bulk phases, respectively. As seen in Figure 5b, the selectivity of CH_3OH over H_2O is approximately 20 at 1 kPa. With increasing pressure, the selectivity decreases gradually as a consequence of entropy (packing) effect. The H_2O molecule is smaller compared to CH_3OH and thus can fit into the channels more effectively at high pressures, leading to a decrease in selectivity. The separation factor of CH_3OH/H_2O by pervaporation was reported to be 3−6 in chitosan membranes within 25−55 °C,[36] and 3−5 in organophilic CMG-OM-010 and 1060-SULZER membranes within 40−70 °C.[37] The substantially higher selectivity at room temperature in the current study suggests that $Zn(BDC)(TED)_{0.5}$ is a promising candidate for the separation of CH_3OH/H_2O vapor and liquid mixtures, or the dehydration of alcohol-based liquid fuels. As demonstrated by the pressure swing adsorption of a CH_3OH/H_2O mixture in $Zn(BDC)(TED)_{0.5}$, the dehydrated CH_3OH could reach 94.7% after the first cycle.[17]

4.2. CO_2/CH_4. Figure 6 shows the isotherms of single-component CO_2 and CH_4 in $Zn(BDC)(TED)_{0.5}$ at 298 K. The experimental data of CO_2 include both adsorption and desorption

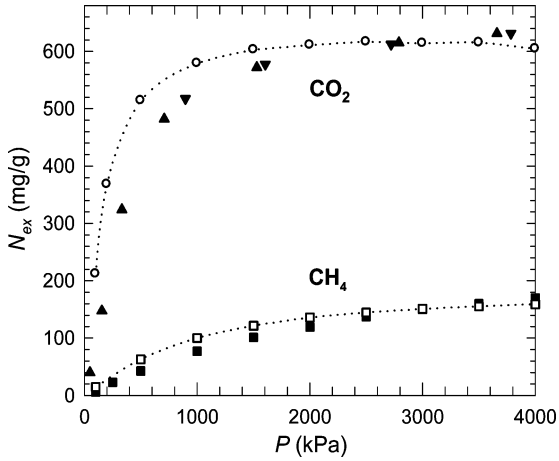

Figure 6. Isotherms of single-component CO_2 and CH_4 at 298 K. The open symbols are simulation results and the filled symbols are experimental data. The upper and lower triangles are experimental adsorption and desorption data of CO_2.

data, which are completely reversible. Fairly good agreement is found between the simulated and experimental results, particularly for CH_4. The overestimation by simulation is attributed to the fact that experimental sample usually contains impurities, which block the channels and reduce the adsorption capacity. CO_2 adsorption is greater than that of CH_4 for two reasons. First, CO_2 has stronger dispersion and electrostatic interactions with the framework. Second, the 298 K temperature considered is subcritical for CO_2 (T_c = 304.4 K), but supercritical for CH_4 (T_c = 190.5 K); that is, CO_2 is substantially more condensable than CH_4 at 298 K. At 3000 kPa, the amount of CO_2 adsorption is about 600 mg/g (13.6 mmol/g) in $Zn(BDC)(TED)_{0.5}$, larger than that in silicalite, carbon nanotube, F-MOF-1, Mn-MOF, and Cu-BTC.[38,39] This is because $Zn(BDC)(TED)_{0.5}$ has a greater free volume, which largely governs adsorption capacity at high pressures.

To identify the adsorption sites for CO_2 in $Zn(BDC)(TED)_{0.5}$, the density contours of CO_2 at 10, 100, and 3000 kPa are shown in Figure 7. The contours here differ remarkably from those of CH_3OH in Figure 3. As discussed above, CH_3OH is a polar molecule and has strong interaction with the metal oxides. However, CO_2 is nonpolar and located preferentially near the BDC linkers as seen on the XZ and YZ planes at 10 kPa. With increasing pressure, further adsorbed CO_2 molecules tend to be near the metal oxides and the TED linkers. At 3000 kPa, the regions between the lateral TED linkers are populated because of the large available space; furthermore, CO_2 is also adsorbed into the small windows. It is interesting to note that compared to CH_3OH, CO_2 enters the small windows more readily because of its linear shape.

As an additional support for the observed shift in the adsorption sites, Figure 8 shows the radial distribution functions of CO_2 around the typical framework atoms at different pressures. With increasing pressure, the peak height in the $g(r)$ around Zn and N atoms rises, which demonstrates the locations of CO_2 move toward the metal oxides at high pressures. The (first) peak height reduces in the $g(r)$ around C2 atoms, but rises in the $g(r)$ around C4 atoms. This indicates that more CO_2 molecules are located near the TED linkers upon increasing pressure, as observed in the density contours.

The simulated adsorption isotherms of an equimolar mixture of CO_2/CH_4 are shown in Figure 9a. CO_2 uptake increases rapidly at low pressures and then becomes saturated with increasing pressure. As a comparison, CH_4 uptake is much smaller and approaches saturation at a low pressure of 500 kPa. The selectivity of CO_2 over CH_4 exhibits similar behavior to the CO_2 isotherm and increases from 4 to 7 with increasing pressure. The increase in selectivity is attributed to the increased intermolecular interactions between adsorbed CO_2 molecules. The selectivity in $Zn(BDC)(TED)_{0.5}$ is similar to that in neutral MOFs such as IRMOF-1, IRMOF-13, IRMOF-14, Cu-BTC, PCN-6, and PCN-6′.[40] Compared to charged *rho*-ZMOF,[15] however, the selectivity in $Zn(BDC)(TED)_{0.5}$ is several orders of magnitude smaller.

In practice, gas mixtures usually contain a small amount of moisture. The presence of H_2O may be adverse to the separation of a gas mixture. For instance, upon the addition of H_2O into a CO_2/CH_4 mixture, the interaction between CO_2 and Na^+ in *rho*-ZMOF is substantially reduced. Consequently, CO_2 adsorption drops and the selectivity decreases by 1 order of magnitude.[41] In other cases, however, the addition of H_2O is beneficial, e.g., the presence of preadsorbed H_2O in BaX zeolite increases the selectivity toward *p*-xylene in *p*-xylene/*m*-xylene mixture.[42] Adsorption of CO_2 and CH_4 in Cu-BTC is enhanced by H_2O molecules coordinated to open metal sites.[43] With a trace amount of H_2O, the selectivity of CO_2/H_2 in *soc*-MOF increases at low pressures due to the promoted adsorption of CO_2 by H_2O bound onto the indium atoms.[14] Similarly, the adsorption of CO_2 and CH_4 and the selectivity of CO_2/CH_4 in mesoporous MIL-101 are enhanced by terminal H_2O molecules.[44]

To examine the effect of H_2O here, the adsorption of a CO_2/CH_4 mixture in the presence of 0.1% H_2O (in terms of mole fraction) was also simulated in $Zn(BDC)(TED)_{0.5}$. As seen in Figure 9a, the addition of H_2O has a marginal effect on the adsorption CO_2 and CH_4 and subsequently the selectivity. The reason, as mentioned above, is that the hydrophobic $Zn(BDC)(TED)_{0.5}$ has very weak affinity for H_2O and the adsorption of H_2O is negligible. This implies that a prewater treatment is probably not required prior to the separation process. Interestingly, the effect of H_2O on the separation of CO_2/CH_4 in $Zn(BDC)(TED)_{0.5}$ is significantly different from that in other MOFs mentioned above, in which a prewater treatment is crucial.

4.3. Hexane. The adsorption of *n*-C_6 in $Zn(BDC)(TED)_{0.5}$ is shown in Figure S3 (Supporting Information). A similar trend is observed in the simulated and experimental isotherms. With increasing pressure, the adsorption increases rapidly at low pressures and then reaches saturation. The saturation capacity is approximately 450 mg/g from simulation, a bit larger than the experimental value of 422 mg/g.[17] The deviation may be attributed to the perfect crystal used in simulation, which has a greater free volume and hence a larger capacity than experiment. The capacity of *n*-C_6 in $Zn(BDC)(TED)_{0.5}$ is exceptionally large due to the highly porous structure and hydrophobic nature, and it is about 2.5 and 3 times larger than in silicalite and cobalt formate MOF, respectively.[45,46] Our simulation results agree well with the simulation results of *n*-C_6 in $Zn(BDC)(TED)_{0.5}$ by Krishna and van Baten.[20] A recent experimental study reported the kinetic separation of C_6 isomers using fixed-bed adsorption.[47] The measured loading of *n*-C_6 is 1 order of magnitude lower than the simulation results. This is probably because of the phase transition or contamination of $Zn(BDC)(TED)_{0.5}$ sample during the adsorption process.

The density contours of *n*-C_6 at 0.001 and 10 kPa are shown in Figure S4 (Supporting Information). Similar to the contours of CO_2, *n*-C_6 interacts strongly with the BDC linkers rather than the metal oxides. Consequently, the preferential site at 0.001 kPa is near the BDC linkers. At 10 kPa, more *n*-C_6 molecules

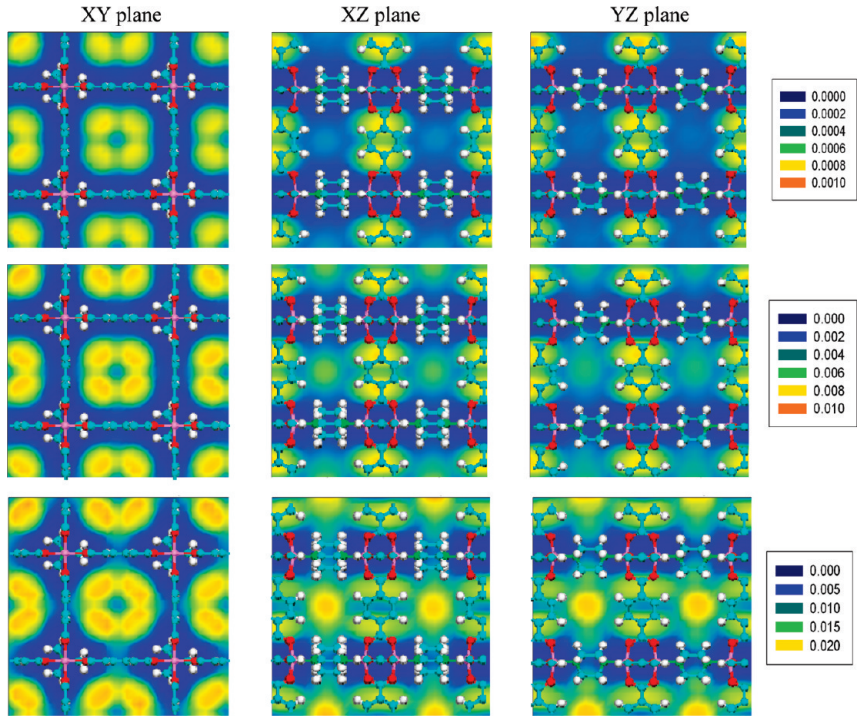

Figure 7. Density contours of CO_2 at 10, 100, and 3000 kPa (from top to bottom). The scale is based on the number of molecules per Å^3.

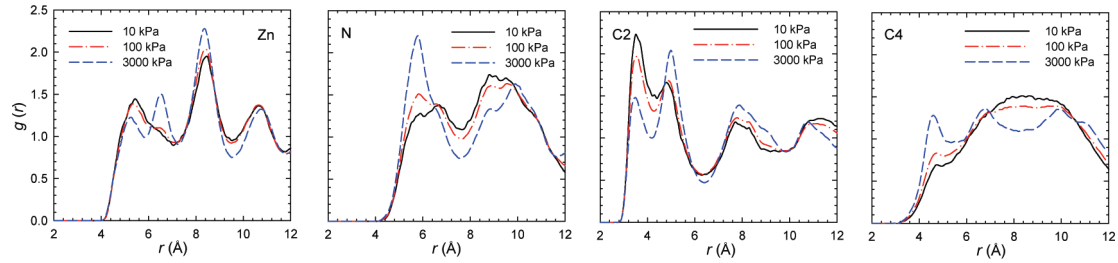

Figure 8. Radial distribution functions of CO_2 around Zn, N, C2, and C4 atoms of $Zn(BDC)(TED)_{0.5}$ at 10, 100, and 3000 kPa. The C2 and C4 atoms are in the BDC and TED linkers, respectively.

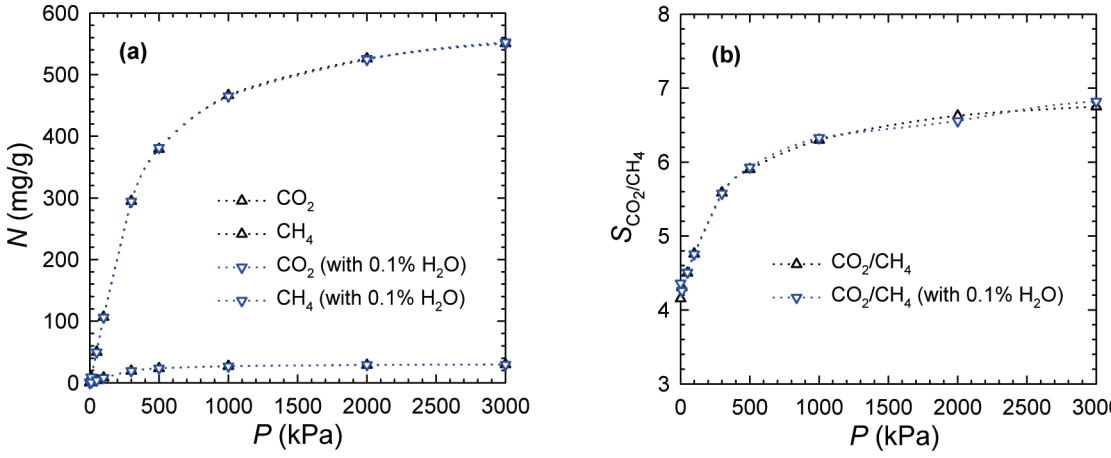

Figure 9. (a) Adsorption and (b) selectivity of an equimolar mixture of CO_2/CH_4 at 298 K.

are adsorbed and located closer to the metal oxides and TED linkers, as also observed in CO_2 adsorption at a high pressure. Compared to CO_2, however, *n*-C_6 is larger in size and cannot extend into the small windows.

5. Conclusions

By integrating experimental and simulation techniques, we have investigated the adsorption and separation of CH_3OH/H_2O and CO_2/CH_4 mixtures in highly hydrophobic $Zn(BDC)(TED)_{0.5}$. The framework contains wide open channels along the *Z* axis, which are connected by the small windows along the *X* and *Y* axes. In general, the simulated isotherms of all pure components (CH_3OH, H_2O, CO_2, CH_4, and *n*-C_6) are in fairly good agreement with experimental results. Because of the hydrophobic BDC and TED linkers, the affinity for H_2O is very weak and thus H_2O adsorption is negligible. The selectivity of

CH_3OH/H_2O is approximately 20 at 1 kPa and decreases gradually with increasing pressure due to entropy effect. The high selectivity at low pressures suggests that $Zn(BDC)(TED)_{0.5}$ could be used for the purification of CH_3OH (or other alcohols) from H_2O. Three favorable adsorption sites are identified in $Zn(BDC)(TED)_{0.5}$ for CH_3OH. At site I near the corner, CH_3OH interacts strongly with the metal oxides and experiences large surface potentials. Sites II and III are less favorable because of the steric hindrance of bulky TED linkers. With increasing pressure, the density distribution in the square channels is less inhomogeneous and the small windows are partially occupied. From the analysis of radial distribution functions, CH_3OH molecules are found to locate closer to the metal oxides at a high pressure.

In contrast to CH_3OH that has strong interaction with the metal oxides, CO_2 is nonpolar and the preferential adsorption site is near the BDC linkers. With increasing pressure, CO_2 molecules are proximal to the metal oxides and TED linkers, and also extend into the small windows. The selectivity of CO_2 over CH_4 increases with increasing pressure, attributed to the increased cooperative interactions of adsorbed CO_2 molecules. In the presence of 0.1% H_2O in CO_2/CH_4 mixture, the adsorption and selectivity remain essentially the same. In other words, H_2O has a negligible effect on the separation of CO_2/CH_4 in $Zn(BDC)(TED)_{0.5}$ and a prewater treatment is perhaps not required.

Acknowledgment. The authors gratefully acknowledge the helpful comments of the anonymous referees, and the financial support from the National University of Singapore (R-279-000-198-112/133 and R-279-000-297-112).

Supporting Information Available: The crystal structure, atomic charges, adsorption isotherms, and density contours of hexane in $Zn(BDC)(TED)_{0.5}$. This material is available free of charge via the Internet at http://pubs.acs.org.

References and Notes

(1) Eddaoudi, M.; Kim, J.; Rosi, N.; Vodak, D.; Wachter, J.; O'Keefe, M.; Yaghi, O. M. *Science* **2002**, *295*, 469.
(2) Yaghi, O. M.; O'Keeffe, M.; Ockwig, N. W.; Chae, H. K.; Eddaoudi, M.; Kim, J. *Nature* **2003**, *423*, 705.
(3) Férey, G. *Chem. Soc. Rev.* **2008**, *37*, 191.
(4) Morris, R. E.; Wheatley, P. S. *Angew. Chem., Int. Ed.* **2008**, *47*, 2.
(5) Lee, J. Y.; Farha, O. K.; Roberts, J.; Scheidt, K. A.; Nguyen, S. T.; Hupp, J. T. *Chem. Soc. Rev.* **2009**, *38*, 1450.
(6) Eddaoudi, M.; Kim, J.; Rosi, N.; Vodak, D.; Wachter, J.; O'Keefe, M.; Yaghi, O. M. *Science* **2002**, *295*, 469.
(7) Millward, A. R.; Yaghi, O. M. *J. Am. Chem. Soc.* **2005**, *127*, 17998.
(8) Garberoglio, G.; Skoulidas, A. I.; Johnson, J. K. *J. Phys. Chem. B* **2005**, *109*, 13094.
(9) Skoulidas, A. I.; Sholl, D. S. *J. Phys. Chem. B* **2005**, *109*, 15760.
(10) Frost, H.; Düren, T.; Snurr, R. Q. *J. Phys. Chem. B* **2006**, *110*, 9565.
(11) Yang, Q. Y.; Zhong, C. L. *J. Phys. Chem. B* **2006**, *110*, 17776.
(12) Martin-Calvo, A.; Garcia-Perez, E.; Castillo, J. M.; Calero, S. *Phys. Chem. Phys. Chem.* **2008**, *10*, 7085.
(13) Bae, Y. S.; Farha, O. K.; Spokoyny, A. M.; Mirkin, C. A.; Hupp, J. T.; Snurr, R. Q. *Chem. Commun.* **2008**, 4135.
(14) Jiang, J. W. *AIChE J.* **2009**, *55*, 2422.
(15) Babarao, R.; Jiang, J. W. *J. Am. Chem. Soc.* **2009**, *131*, 11417.
(16) Dybtsev, D. N.; Chun, H.; Kim, K. *Angew. Chem., Int. Ed.* **2004**, *43*, 5033.
(17) Lee, J. Y.; Olson, D. H.; Pan, L.; Emge, T. J.; Li, J. *Adv. Funct. Mater.* **2007**, *17*, 1255.
(18) Liu, J.; Lee, J. Y.; Pan, L.; Obermyer, R. T.; Simizu, S.; Zande, B.; Li, J.; Sankar, S. G.; Johnson, J. K. *J. Phys. Chem. C* **2008**, *112*, 2911.
(19) Dubbeldam, D.; Galvin, C. J.; Walton, K. S.; Ellis, D. E.; Snurr, R. Q. *J. Am. Chem. Soc.* **2008**, *130*, 10884.
(20) Krishna, R.; van Baten, J. M. *Mol. Simul.* **2009**, *35*, 1098.
(21) Krishna, R.; van Baten, J. M. *Chem. Eng. Sci.* **2009**, *64*, 3159.
(22) *Materials Studio*, 4.3 ed.; Accelrys, Inc.: San Diego, CA, 200.
(23) Smart, O. S.; Neduvelil, J. G.; Wang, X.; Wallace, B. A.; Sansom, M. S. P. *J. Mol. Graphics Model.* **1996**, *14*, 354.
(24) Myers, A. L.; Monson, P. A. *Langmuir* **2002**, *18*, 10261.
(25) Frisch, M. J.; Trucks, G. W.; Schlegel, H. B.; Scuseria, G. E.; Robb, M. A.; Cheeseman, J. R.; Zakrzewski, V. G.; Montgomery, J. A.; Stratmann, R. E.; Burant, J. C.; Dapprich, S.; Millam, J. M.; Daniels, A. D.; Kudin, K. N.; Strain, M. C.; Farkas, O.; Tomasi, J.; Barone, V.; Cossi, M.; Cammi, R.; Mennucci, B.; Pomelli, C.; Adamo, C.; Clifford, S.; Ochterski, J.; Petersson, G. A.; Ayala, P. Y.; Cui, Q.; Morokuma, K.; Malick, D. K.; Rabuck, A. D.; Raghavachari, K.; Foresman, J. B.; Cioslowski, J.; Ortiz, J. V.; Stefanov, B. B.; Liu, G.; Liashenko, A.; Piskorz, P.; Komaromi, I.; Gomperts, R.; Martin, R. L.; Fox, D. J.; Keith, T.; Al-Laham, M. A.; Peng, C. Y.; Nanayakkara, A.; Gonzalez, C.; Challacombe, M.; Gill, P. M. W.; Johnson, B. G.; Chen, W.; Wong, M. W.; Andres, J. L.; Head-Gordon, M.; Replogle, E. S.; Pople, J. A. *Gaussian 03*; Revision D.01 ed.; Gaussian, Inc., Wallingford, CT, 2004.
(26) Singh, U. C.; Kollman, P. A. *J. Comput. Chem.* **1984**, *5*, 129.
(27) Mayo, S. L.; Olafson, B. D.; Goddard, W. A. *J. Phys. Chem.* **1990**, *94*, 8897.
(28) Jorgensen, W. L.; Chandrasekhar, J.; Madura, J. D.; Impey, R. W.; Klein, M. L. *J. Chem. Phys.* **1983**, *79*, 926.
(29) Mark, P.; Nilsson, L. *J. Phys. Chem. A* **2001**, *105*, 9954.
(30) Hirotani, A.; Mizukami, K.; Miura, R.; Takaba, H.; Miya, T.; Fahmi, A.; Stirling, A.; Kubo, M.; Miyamoto, A. *Appl. Surf. Sci.* **1997**, *120*, 81.
(31) Martin, M. G.; Siepmann, J. I. *J. Phys. Chem. B* **1998**, *102*, 2569.
(32) Chen, B.; Potoff, J. J.; Siepmann, J. I. *J. Phys. Chem. B* **2001**, *105*, 3093.
(33) Greathouse, J. A.; Kinnibrugh, T. L.; Allendorf, M. D. *Ind. Eng. Chem. Res.* **2009**, *48*, 3425.
(34) *NIST Chemistry WebBook*; Linstrom, P. J., Ed.;National Institute of Standards and Technology: Washington, DC, 2010.
(35) Nalaparaju, A.; Babarao, R.; Zhao, X. S.; Jiang, J. W. *ACS Nano* **2009**, *3*, 2563.
(36) Won, W.; Feng, X.; Lawless, D. *J. Membr. Sci.* **2002**, *209*, 493.
(37) Molina, J. M.; Vatai, G.; Bekassy-Molnar, E. *Desalination* **2002**, *149*, 89.
(38) Babarao, R.; Jiang, J. W. *Langmuir* **2008**, *24*, 6270.
(39) Yang, Q. Y.; Zhong, C. L.; Chen, J. F. *J. Phys. Chem. C* **2008**, *112*, 1562.
(40) Babarao, R.; Jiang, J. W.; Sandler, S. I. *Langmuir* **2009**, *25*, 5239.
(41) Babarao, R.; Jiang, J. W. *Energy Environ. Sci* **2009**, *2*, 1088.
(42) Moise, J. C.; Bellat, J. P. *J. Phys. Chem. B* **2005**, *109*, 17239.
(43) Yazaydin, A. O.; Benin, A. I.; Faheem, S. A.; Jakubczak, P.; Low, J. J.; Willis, R. R.; Snurr, R. Q. *Chem. Mater.* **2009**, *21*, 1425.
(44) Chen, Y. F.; Babarao, R.; Sandler, S. I.; Jiang, J. W., *Langmuir*. DOI: 10.1021/la904502h. Published Online: Jan 27, 2010.
(45) Vlugt, T. J. H.; Krishna, R.; Smit, B. *J. Phys. Chem. B* **1999**, *103*, 1102.
(46) Li, K.; Olson, D. H.; Lee, J. Y.; Bi, W.; Wu, K.; Yuen, T.; Xu, Q.; Li, J. *Adv. Funct. Mater.* **2008**, *18*, 2205.
(47) Barcia, P. S.; Zapata, F.; Silva, J. A. C.; Rodrigues, A. E.; Chen, B. L. *J. Phys. Chem. B.* **2007**, *111*, 6101.

JP1003177

Supporting Information

A Highly Hydrophobic Metal-Organic Framework $Zn(BDC)(TED)_{0.5}$ for Adsorption and Separation of CH_3OH/H_2O and CO_2/CH_4: An Integrated Experimental and Simulation Study

Y. F. Chen,[†] J. Y. Lee,[‡] R. Babarao,[†] J. Li,[‡] J. W. Jiang[†*]

[†]*Department of Chemical and Biomolecular Engineering, National University of Singapore, 117576, Singapore,* [‡]*Department of Chemistry and Chemical Biology, The State University of New Jersey, Piscataway, New Jersey 08854*

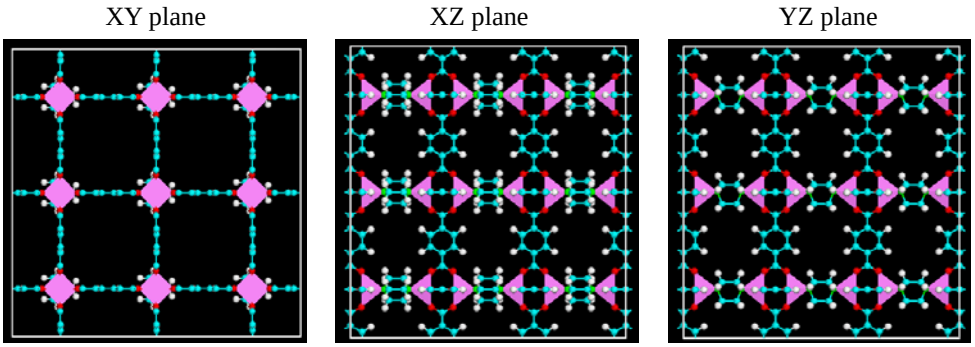

Figure S1. Crystal structure of $Zn(BDC)(TED)_{0.5}$ constructed from experimental crystallographic data and first-principles optimization. Color code: Zn, pink polyhedra; N, green; C, cyan; O, red; H, white.

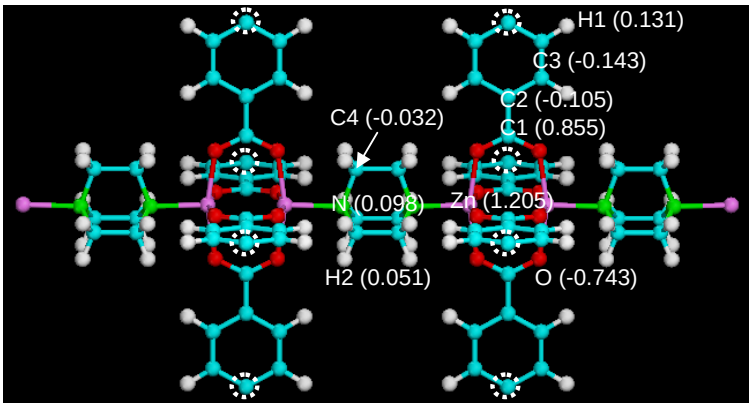

Figure S2. Atomic charges in a fragmental cluster of $Zn(BDC)(TED)_{0.5}$ from density functional theory. The dangling bonds (indicated by circles) were terminated by hydrogen atoms. Color code: Zn, pink; N, green; C, cyan; O, red; H, white.

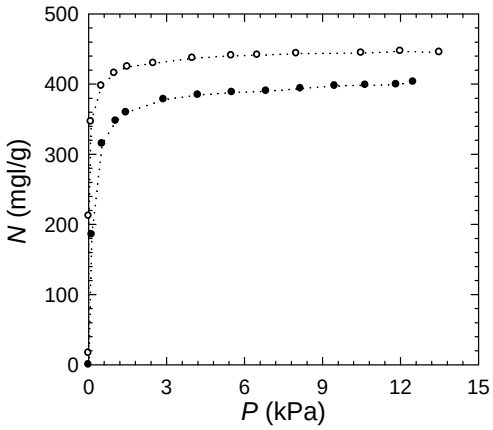

Figure S3. Adsorption of hexane at 313 K in Zn(BDC)(TED)$_{0.5}$. The open symbols are simulation results and the filled symbols are experimental data.

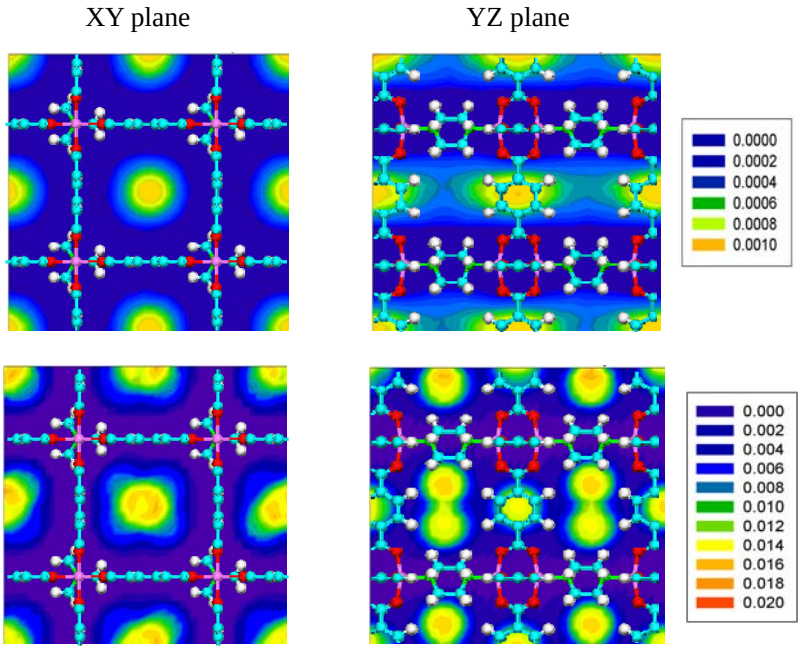

Figure S4. Density contours of hexane in Zn(BDC)(TED)$_{0.5}$ at 0.001 kPa (top) and 10 kPa (bottom). The scale is based on the number of molecules per Å^3.